Research article

LUMINESCENCE
The Journal of Biological and Chemical Luminescence

Received: 17 January 2016, Revised: 25 March 2016, Accepted: 26 March 2016 Published online in Wiley Online Library

(wileyonlinelibrary.com) DOI 10.1002/bio.3149

Fluorescent carbon nanoparticles from *Citrus sinensis* as efficient sorbents for pollutant dyes

Oluwaseun Adedokun,[a,b]* Anurag Roy,[a] Ayodeji O. Awodugba[b] and P. Sujatha Devi[a]*

ABSTRACT: Here, we report a simple, green and economic process for the synthesis of highly fluorescent carbon nanoparticles (CPs) through low-temperature carbonization of a fruit waste, *Citrus sinensis* peel. This approach allows the large-scale production of aqueous CPs dispersions without any additives and post-treatment processes. The as-prepared CPs were of small particle size, exhibited bright blue fluorescence under UV irradiation (λ_{max} = 365 nm) with excellent colloidal stability in water. The chemical composition, structure and morphology of the as-prepared CPs were analyzed using various spectroscopic techniques such as X-ray diffraction, transmission electron microscopy and raman spectroscopy. The formed CPs were turbostratic in nature, with a large number of functional groups on the surface. We explored the adsorption characteristics of the formed CPs for wastewater treatment. Because of the negative surface of the CPs, as evident from the zeta value, it is possible to use them for selective adsorption of the cationic dye methylene blue from a mixture of dyes. The equilibrium adsorption isotherm revealed that the Langmuir model better describes the adsorption process than the Freundlich model. As-prepared CPs rapidly adsorbed ~84% of the methylene blue within 1 min and can be regenerated and used repeatedly. Copyright © 2016 John Wiley & Sons, Ltd.

Additional supporting information may be found in the online version of this article at the publisher's web site.

Keywords: Citrus sinensis; turbostratic carbon; cationic dye; adsorption efficiency; selective adsorption

Introduction

Fluorescent carbon nanoparticles (CPs), a new class of emerging carbon material, have attracted significant attention due to their fascinating properties, which include high photostability, tunable optical properties, high chemical stability, easy functionalization, low cytotoxicity and, above all, high biocompatibility (1,2). Some CPs have potential application in bioimaging (3,4), optoelectronic devices (1), photocatalysis (5), wastewater treatment (6) and in sensors (7). Many synthetic routes for fluorescent CPs have been explored, such as laser ablation, arc-discharge, acid dehydration, electrochemical oxidation, hydrothermal reaction and microwave heating (8–10). Some of these synthesis techniques require high-value equipment, non-environmentally friendly chemicals, catalysts or harsh experimental conditions, which increase production costs. Because of these disadvantages, the development of simple and green preparative strategies for fluorescent CPs is in high demand. As a result, there are ongoing efforts to develop simple, direct and economical methods to synthesize carbon nanoparticles without any surface passivation (5,6,9,11). Among these strategies, the thermal (combustion) supported route, also known as pyrolysis of carbonaceous precursors, is a simple, clean and cost-effective method. Many researchers have demonstrated the success of thermal degradation of various naturally occurring materials through furnace and microwave-assisted pyrolysis (6,8,12,13).

Various functional carbon materials can be synthesized from abundant natural biomass waste, which is cost-effective, non-toxic and easily available. In view of increasing global awareness of the need for a clean and green environment through waste reduction, the choice of reusing or recycling carbon-rich waste as a starting material for CP synthesis is an added advantage. In addition, biomass wastes are renewable and cost-effective resources, and some natural biomass wastes have been shown to be suitable starting precursors for the synthesis of CPs (6–9,11). In general, natural biomass contains different components, such as starch, cellulose, hemicellulose and lignin, together with micro amounts of extractives and minerals (14,15). Although, fluorescent CPs from natural biomass sources have been studied for application in photocatalysts (16), sensors (17,18) and bioimaging (3,4,19), the use of fluorescent CPs from an orange peel precursor as an adsorbent for wastewater treatment has rarely been reported.

Here, we report a simple, green and economic process for the synthesis of highly fluorescent CPs by low-temperature carbonization of fruit waste, namely orange (Citrus sinensis) peel. Thermal decomposition of orange peel led to the formation of fluorescent CPs with excellent adsorption characteristics toward water-polluting dye molecules.

Experimental

Chemicals

Fresh fruits of Citrus sinensis (orange) were bought from a local farm in Ogbomoso, Nigeria. Methylene blue (MB) and methylene

* Correspondence to: P. S. Devi, Sensor and Actuator Division, CSIR-Central Glass and Ceramic Research Institute, 196, Raja SC Mullick Road, Jadavpur, Kolkata 700 032, India. E-mail: psujathadevi@cgcri.res.in

* O. Adedokun, Department of Pure and Applied Physics, Ladoke Akintola University of Technology, P.M.B 4000, Ogbomoso, Nigeria. E-mail: oadedokun@lautech.edu.ng

[a] Sensor and Actuator Division, CSIR-Central Glass and Ceramic Research Institute, 196, Raja SC Mullick Road, Jadavpur, Kolkata 700 032, India

[b] Department of Pure and Applied Physics, Ladoke Akintola University of Technology, P.M.B 4000 Ogbomoso, Nigeria

orange (MO) (Sigma-Aldrich, India) were used as received. Distilled water was used as the medium throughout. All chemicals were of analytical grade (AR) and were used without further purification.

Preparation of CPs

Fresh Citrus sinensis fruits were used as the raw material. The peel was removed and washed with distilled water, followed by vacuum-drying at 60 °C for 24 h. The dried peels were then crushed to a fine powder. CPs were prepared by low-temperature carbonization of fruit peel. In a typical procedure, 5 g of fine powder was carbonized at mild constant temperature of 220 °C in a furnace for 2 h in air (Scheme 1). A dark brown product was obtained after allowing it to cool naturally at room temperature. The obtained product was dispersed in 100 mL of distilled water, homogenized under sonication for 15 min and then centrifuged at 12,000 rpm for 10 min. The resultant supernatant containing CPs was dried under vacuum for 24 h. The overall yield of CPs, calculated from the weight of the powdery raw material and the final weight of the product formed was 15.08 ± 0.5%. CPs were finally dispersed in distilled water at a concentration of 0.25 mg/L for optical studies.

Instrumentation

To study the thermal decomposition of the precursor, thermogravimetric analysis (TGA) was carried out on the powder samples from room temperature to ~1000 °C at a heating rate of 10 °C/min on a NETZSCH STA 449 C simultaneous TGA–DTA analyzer (Germany). The dried powder was further characterized by powder X-ray diffraction (XRD) analysis on a X'pert pro MPD XRD of PAN analytical with CuKα radiation (λ = 1.5406 Å). Fourier transform infrared (FTIR, Netherlands) spectra of the samples were measured within the interval of 400 and 4000 cm^{-1} on a NICOLET 380 FTIR spectrometer (Waltham, Massachusetts) using potassium bromide (KBr) powder. Raman signals were obtained using a STR500, Cornes Technologies Raman spectrometer (Japan) with an excitation of 514.5 nm from an argon ion green laser (50 mW). The Raman signals were measured at different exposure times (5 s, 10 s) and different data acquisition times. The microstructure of the CPs was analyzed by transmission electron microscopy (TEM; Tecnai G^2 30ST high-resolution transmission electron microscope Netherlands operating at an acceleration voltage of 300 kV). The sample was prepared by dropping a given volume of a well-dispersed CP solution onto a carbon-coated copper grid followed by drying in air. The spectroscopic properties of the CPs were studied using a UV/Vis/NIR (near infra red) spectrophotometer (Shimadzu UV-3600) and spectrofluorometer (QM-40, Photon Technology International, Bimingham Road, New Jersey) with a 150 W xenon lamp as the excitation source. The zeta potential was recorded using a Horiba Nanoparticle Analyzer SZ100 (Japan).

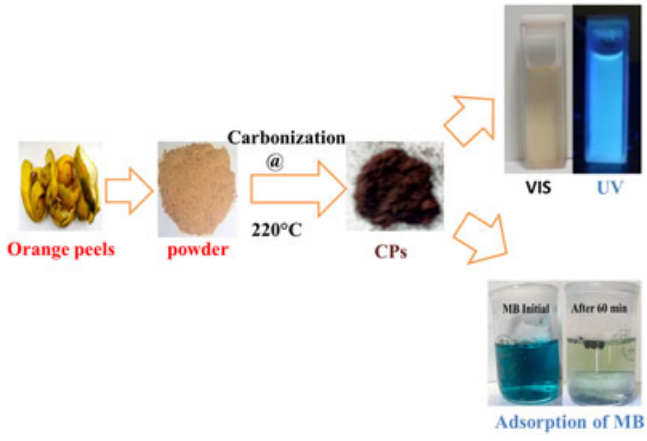

Scheme 1. Schematic representation of synthesis of fluorescent CP from waste orange peel and its application towards removal of MB dye.

Adsorption experiment

Adsorption experiments were performed at room temperature. In detail, to 10 mL of a known concentration of MB dye was added 10 mg of CPs powder in an experimental beaker. To study the effect of equilibrating homogenization of the solution on the adsorption, three methods were employed, viz. stirring at 150 rpm for 45 min, initial sonication for 5 min followed by stand-alone (in separate experiments). The solution pH was adjusted with HCl (0.1 M) or NaOH (0.1 M), and was measured using a Sartorius PB-11 pH meter (Bohemia, New York). Samples were removed from the beaker at predetermined time intervals until adsorption equilibrium was achieved. The dye solution was separated from the adsorbent by centrifugation at 8000 rpm for 5 min before measuring the residual dye concentration. The residual MB concentration was calculated by Beer's law and a standard curve based on the maximum absorption band at 665 nm using an UV/Vis/NIR spectrophotometer. The dye removal efficiency and among of adsorption were evaluated based on the difference in the MB concentration in the aqueous solution before and after adsorption, according to equations 1 and 2 below (20):

$$(\%)\ Dye\ removal = \frac{C_o - C_e}{C_o} \times 100 \quad (1)$$

$$Q_e = \frac{(C_o - C_e) \times V}{W} \quad (2)$$

where Q_e (mg/g) is the amount of dye adsorbed per gram of adsorbent at equilibrium, C_o (mg/L) is the initial concentration of dye in the solution, C_e (mg/L) is the equilibrium concentration at time, t (min), V (L) is the volume of solution and W (g) is the mass of adsorbent used.

Selective adsorption of cationic dye from a mixture of dyes

Selective adsorption experiments were performed with a mixture of MB and MO at pH 6.5. In a typical experiment, 10 mg of powdered CPs was added to 10 mL of a mixed solution of MB and MO having initial concentrations of 10^{-5} M each. After stirring at 150 rpm and room temperature for 45 min, the dye solution was separated by centrifugation. The dye concentration in the solution and the removal of dye were monitored and evaluated by UV/vis spectra.

Desorption experiments

Regeneration of the adsorbents was performed with a mixture of methanol and acetic acid (9:1 v/v). Saturated CPs were added to a mixture of methanol and acetic acid at a ratio of 5 g/L, and the suspension was left for 2 h. Subsequently, the CPs were collected by centrifugation. After washing with water and air drying, the CPs were regenerated and reused for adsorption. The adsorption/desorption of the MB onto/from the CPs was assessed for five consecutive cycles.

LUMINESCENCE
The Journal of Biological and Chemical Luminescence

Results and discussion

The TGA study on powdered orange peel was conducted to understand the thermal decomposition characteristics of the precursor. A typical thermal analysis of the precursor powder, obtained from TG–DTA in dry air, is shown in Fig. 1(a). From the thermal profile, four main thermal events can be clearly distinguished up to 500 °C. It is observed that the mass of dry orange peel powder decreases continuously between room temperature and 520 °C, which is attributed to dehydration and thermal degradation of the powder. The initial 5.28% loss of mass, below 100 °C, is associated with the release of weakly bonded water molecules. In addition, the main losses of mass at 210, 312 and 468 °C were associated with decomposition of the biomass into its three main components (hemicellulose, cellulose and lignin, respectively) (21). All the thermal events were typically exothermic in nature, except the water release at 80 °C. After the desorption of physically bonded water, the dehydrated biomass was stable up to 145 °C, and then began to decompose. The first step from 155 to 260 °C, characterized by an exothermic peak at 210 °C, coincides with a 24.72% loss of mass and is attributed to the degradation of hemicellulose. Hemicellulose is a mixture of various polymerized monosaccharides, such as glucose, mannose, galactose, xylase and arabinose among others, with low molecular mass and lower thermal stability than cellulose (22). Hemicellulose decomposes between 200 and 260 °C, giving rise to more volatiles, fewer tars, and fewer chars than cellulose (14). In the simultaneous processes between 265 and 370 °C, an exothermic peak is seen at 312 °C, associated with a 33.50% loss of mass due to the degradation of cellulose. Cellulose forms long chains that are bonded to each other by a long network of hydrogen bonds. As a consequence of their crystalline structure, they resist thermal degradation better than the hemicelluloses (14,21). During the last stage, over a temperature range of 400–520 °C, an exothermic peak is identified at 468 °C. The total loss of mass up to 520 °C relative to the initial mass at this last stage was 24.50%. This may be attributed to the degradation of lignin and char residue, in which homologous phenolic compounds might be the main product (14). Lignin is an amorphous cross-linked resin with no exact structure and its degradation occurs between 280 and 500 °C (22). Based on thermal decomposition studies, the calcination temperature was fixed to produce highly fluorescent CPs from the biomass.

Figure 1(b) shows the typical XRD profile of as-prepared CPs. The broad peaks at 24.3° and 37.8° are assigned to the (002) and (101) planes, respectively, of turbostratic carbon (11). The peak at 24.3° corresponding to an interlayer spacing (*d*) of 3.66 Å is slightly higher than the 002 plane spacing of the graphitic carbon (3.44 Å). This increase in *d* indicates an increase in the amorphous nature and is attributed to the introduction of more oxygen-containing groups (11). This can be further confirmed by the selected area electron diffraction (SAED) pattern of the CPs shown in Fig. 2(c). The FTIR spectrum displays the functional groups associated with the as-prepared CPs. Figure 1(c) shows a characteristic broad OH peak at 3440 cm^{-1}, whereas the distinctive band at 2924 cm^{-1} is related to the presence of C–H stretching vibrations, together with bending vibrations around 1399 cm^{-1} (22). The absorption peak at 1730 cm^{-1} is ascribed to C = O stretching modes, indicating the existence of carboxyl groups. The signal at 1632 cm^{-1} is due to C = C stretching and asymmetric and symmetric stretching vibrations of C–O–C around 1264 cm^{-1}. The data confirm the presence of hydrophobic C = C moieties and hydrophilic oxygen-containing functional groups in the as-prepared CPs. The presence of a broad D-band at 1380 cm^{-1}, G-band at 1589 cm^{-1} and 2D-band at 2974 cm^{-1} in the Raman spectrum,

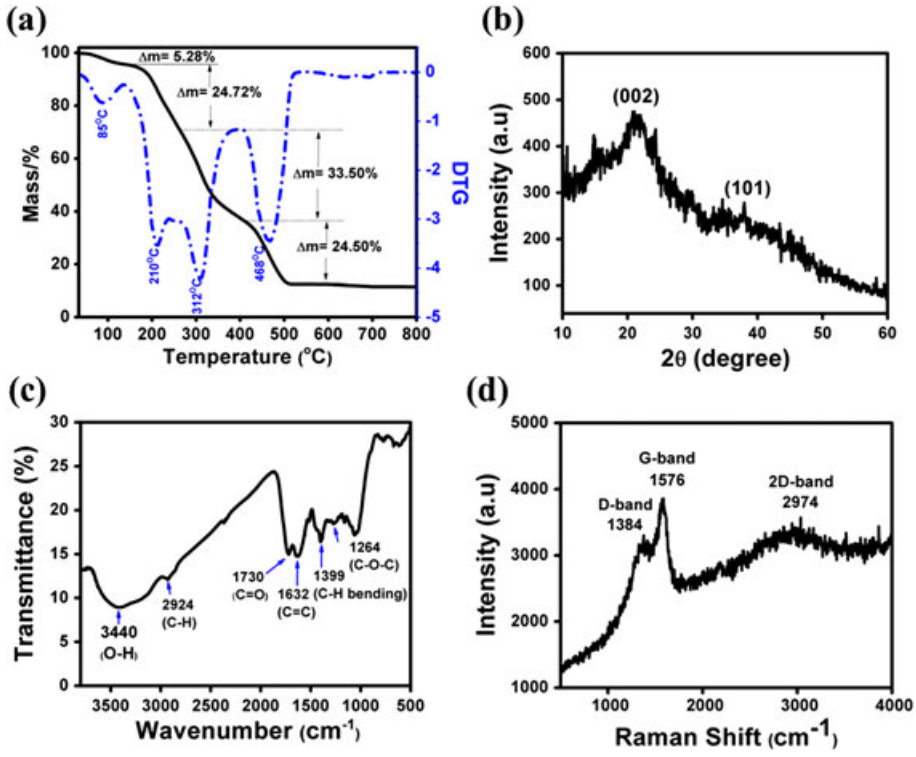

Figure 1. (a) DTA–TG plot of the precursor powder in air at a heating rate of 10 °C/min. (b) XRD pattern of the as-prepared CPs. (c) FTIR spectrum of the as-prepared CPs and (d) Raman spectrum of the as-prepared CPs.

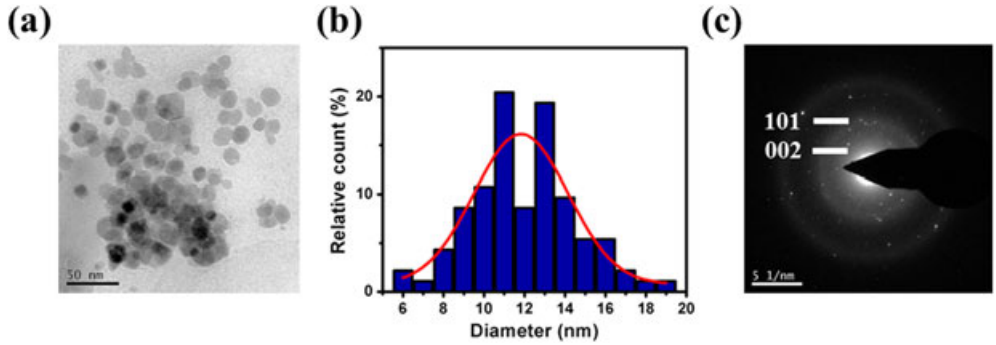

Figure 2. (a) TEM image of the as-prepared CPs. (b) Corresponding size distribution histogram. (c) SAED pattern of the CPs.

shown in Fig. 1(d), indicates the graphitic nature of the CPs. The relative intensity of $\frac{I_D}{I_G}$ is 0.848. The zeta potential of the CPs was −38.9 mV (Fig. S1). This confirms the formation of functionalized CPs with hydroxyl and carboxyl moieties on the surface.

The TEM bright field image in Fig. 2(a) vividly reveals that the CPs are spherical in shape with a wide size distribution in the range of 6.0–19.0 nm (average size 11.0 nm) as confirmed from the size distribution histogram shown in Fig. 2(b).

In order to explore the optical characteristics of the as-prepared CPs, UV/vis spectroscopy of the sample was recorded, as shown in Fig. 3(a). The UV/vis absorption spectrum of CPs displays a weak absorption band at around 280 nm, which is typically ascribed to the presence of aromatic π orbitals (5,10). As-prepared CPs in aqueous solution show blue luminescence upon exposure of UV light, as shown in the inset to Fig. 3(a). The maximum photoluminescence was observed around 450 nm upon excitation at 360 nm. The full-width at half-maximum (FWHM) at the strongest photoluminescence maximum for CPs was evaluated to be 100 nm, which was relatively broad compared with those reported in the literature (< 100 nm) (7,18). This suggests that as-prepared CPs have a broad distribution of particle sizes, which correlates well with the TEM analysis. The synthesized CPs also exhibited excitation-dependent emission, as shown in Fig. 3(b). CPs exhibit excitation-dependent emission due to the presence of trap states arising from the surface defects (1,3,4,6,8,10). We also studied the optical properties of the fruit extract derived from the powder sample of the precursor, as shown in Fig. 3(c). It is speculated that the sample extracts contain chlorophyll-derivative and

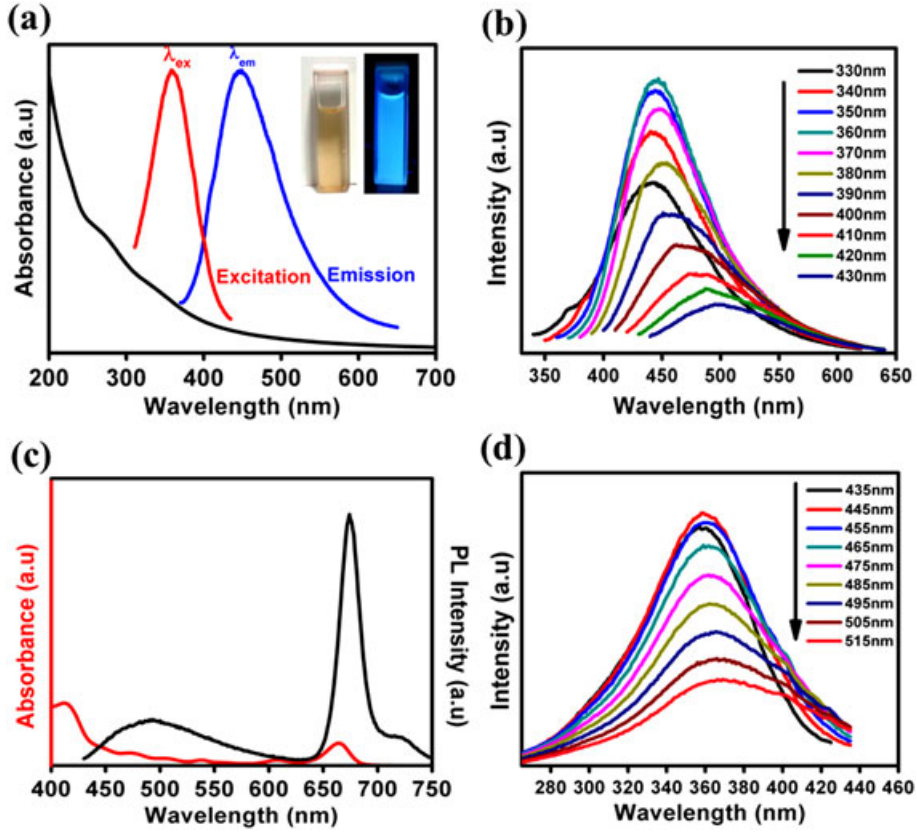

Figure 3. (a) UV absorption, excitation and emission spectra. (Inset) Optical image under daylight and UV light. (b) Emission spectra at different excitation wavelengths in 10 nm increments. (c) Optical absorption and emission spectra of orange peel extract before carbonization. (d) Excitation spectra of extract at different emission wavelengths in 10 nm increments.

LUMINESCENCE
The Journal of Biological and Chemical Luminescence

non-chlorophyll-derivative pigments. It is interesting to find the red emission from the fruit extract, compared with the blue emission from the calcined fruit extract powder (20).

MB, a cationic dye was chosen as a model dye to evaluate the adsorption ability of CPs (21). The chemical structure of MB has rich aromatic ring and a cationic atom (S^+), which is favorable for adsorbing on the CPs surface through π–π staking and ionic interaction. We evaluated the adsorption efficiency of MB dye under different conditions such as stirring at 150 rpm for 45 min, 5 min sonication and the stand-alone method at room temperature with an MB concentration of 10^{-5} M. The removal rate was quite rapid (within 1 min) for both stirring and sonication, but slow in the stand-alone condition, as shown in Figs 4(a) and S3. The removal efficiency was calculated as 97%, 85% and 59% for stirring, 5 min initial sonication and the stand-alone method, respectively (Fig. S3). This is because, initially on stirring at 150 rpm and 5 min initial sonication, the diffusion rate of MB dye from the bulk liquid to the liquid boundary layer surrounding the CPs adsorbent increases due to enhanced turbulence. This results in a higher adsorption efficiency. The above results confirm that stirring at 150 rpm is sufficient for the rapid adsorption of MB dye to the CPs surface. Therefore, we maintained this condition (stirring at 150 rpm) for further experiments. It is worth mentioning that ~84% of the MB dye could be removed from water by the CPs adsorbent within 1 min. We speculate that the strong adsorption characteristic of CPs is due to strong ionic interactions between the negatively charged surface COO^- groups and the positively charged functional groups of the dye molecule.

However, the pH of the dye solution may affect the aqueous chemistry and surface binding sites of ionic-type adsorbents. To gain further insight into the adsorption process, the effect of initial pH on the adsorption efficiency of CPs was studied for pH values of 1, 3, 5, 7, 9, and 11 at room temperature, an initial dye concentration of 10^{-5} M with an adsorbent dose of 10 mg and a contact time of 45 min.

Figure 4(b) shows the removal efficiency of CPs for MB at various pH values. On increasing the pH from 3 to 7, the dye removal ability of CPs for MB gradually increases. This is attributed to the fact that the variation in pH influences the surface charges of CPs and the degree of ionization of the dyes. The CPs adsorbent is negatively charged in solution due to the presence of many carboxylic groups. The decrease in removal efficiency at very low pH is possibly caused by the competition of protons with dye molecules for the available adsorption sites. As the pH increases, the electrostatic attraction between the negatively charged surface of CPs and cationic MB molecule enhances, resulting into increase in removal efficiency of adsorbent.

More often in practical applications, the contact time required to reach equilibrium is an important parameter. To establish the time-dependent adsorption, the adsorption of MB dye on CPs as a function of contact time, the dye removal efficiency and the adsorption capacity of CPs at different contact times were evaluated experimentally. As shown in Fig. 4(c,d), the adsorption rate for MB initially increased rapidly over 1 min, and then slowed until the process reached equilibrium within just 30 min. Approximately 84% of the MB could be adsorbed within the first 1 min. This initial rapid dye adsorption is caused by surface electrostatic attraction on the CPs surface because of the existence of a large number of adsorption sites. The later slow step is attributed to the limited

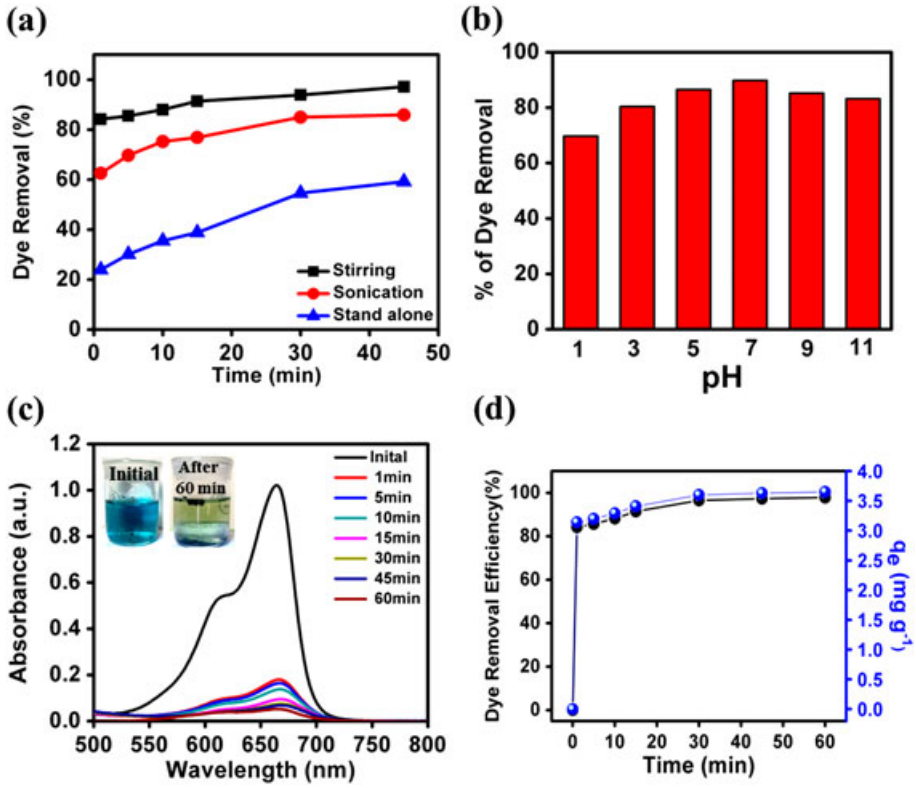

Figure 4. (a) Removal efficiency of MB dye from an aqueous solution by CPs using different methods with different uptake times. (b) Effect of pH on the efficiency of dye removal. (c) UV/vis absorbance spectra of the separated MB solution at different uptake times. (Inset) MB initially and after 60 min. (d) Dye removal efficiency and adsorption rate of MB dye removal at 10^{-5} M.

adsorption sites available on the surface of CPs, and the adsorption process followed intraparticle diffusion. The adsorption kinetics and isotherms were investigated to understand the adsorption process.

Adsorption kinetics

In order to investigate the adsorption mechanism, the pseudo-first-order and pseudo-second-order were verified by the linear expression: $\log(q_e - q_t)$*vs t*, $\frac{t}{q_t}$ *vs t*.

The pseudo-first-order model describes the adsorption of a solute from an aqueous solution (23). The pseudo-first-order model is represented below:

$$\log(q_e - q_t) = \log q_e - \frac{K_1}{2.303}\, t \tag{3}$$

where q_e and q_t (mg/g) are the amount of MB adsorbed at equilibrium and time t (min), respectively, and $K_1(\text{min}^{-1})$ is the pseudo-first-order rate constant.

The pseudo-second-order model is based on the adsorption capacity of the solid phase (23). The model is expressed as:

$$\frac{t}{q_t} = \frac{1}{K_2 q_e^2} + \frac{t}{q_e} \tag{4}$$

Where, K_2 is the pseudo-second-order rate constant (g/mg/min).

Figure 5(a,b) shows a plot of the pseudo-first-order and pseudo-second-order kinetic models at different initial MB dye concentrations. Table 1 gives the rate constants of the two models with their correlation coefficients. It is obvious that at low concentrations the pseudo-first-order and pseudo-second-order fit well with our experimental data, whereas at relatively high concentrations, the pseudo-second-order is more suitable for describing the adsorption process, as evident from the correlation coefficient. Based on our observations, as the dye concentration increases, there is tendency for the pseudo-first-order kinetic model to be poorly correlated with the experimental adsorption data.

Intraparticle diffusion model

To further evaluate the step controlling the adsorption process of MB onto CP adsorbents, we used the intraparticle diffusion model (24) which can be expressed as:

$$q_t = K_i t^{0.5} + C \tag{5}$$

where K_i is the intraparticle rate constant and C is the intercept. As speculated, the plot of q_t vs. $t^{0.5}$ was a straight line, and the adsorption process should involve intraparticle diffusion. In addition, the line passed through the origin, and so particle diffusion was the controlling step. The intraparticle diffusion kinetics for the adsorption of MB onto CPs at different MB dye concentrations is shown in Fig. 5(c,d), and could be divided into three stages. The first stage was rapid adsorption that occurred within first 1 min and is attributed to external surface adsorption, that is, MB dye molecules diffused through the bulk solution to the external surface of the adsorbent. The second stage was a gradual adsorption process, in which intraparticle diffusion was rate controlling. Thereafter, the adsorption of MB onto CPs became very slow and stable, reaching equilibrium and maximum adsorption, similar to the results reported by Wang et al. (25).

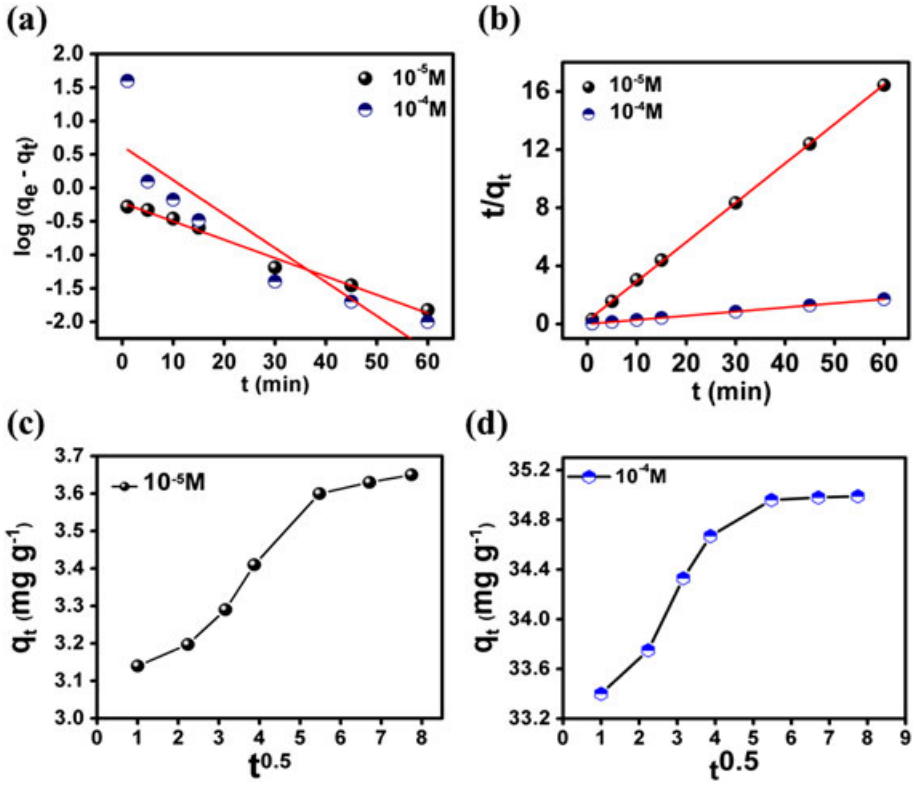

Figure 5. (a) Pseudo-first-order kinetic and (b) pseudo-second-order kinetic plot for the adsorption of MB at different initial concentrations. (c, d) Intraparticle diffusion kinetics for the adsorption of MB onto CPs at initial concentrations of 10^{-5} M (c) and 10^{-4} M.

LUMINESCENCE
The Journal of Biological and Chemical Luminescence

Table 1. The obtained parameters for pseudo first-order and pseudo second-order kinetic model and their coefficient of correlation

	Pseudo first-order kinetic model			Pseudo second-order kinetic model		
C_o (M)	q_e (mg/g)	K_1 (min^{-1})	R^2	q_e (mg/g)	K_2 (g/min/mg)	R^2
10^{-5}	3.665	0.518	0.9856	4.590	0.175	0.9997
10^{-4}	35.014	1.436	0.7735	234.74	6.368×10^{-4}	0.9999

Adsorption isotherm

The adsorption isotherm describes how the adsorbate molecules are distributed between the liquid phase and solid phase. We used two common models in this study, viz. the Langmuir and Freundlich isotherm models, to describe the experimental data. The linear forms of Langmuir and Freundlich isotherm models (26,27) are expressed in equations 6 and 7, respectively,

$$\frac{C_e}{q_e} = \frac{C_e}{q_{max}} + \frac{1}{q_{max} K_L} \quad (6)$$

$$\ln q_e = \ln K_F + b_F \ln C_e \quad (7)$$

where K_F((mg/g) is the Freundlich constant, b_F (g/mL) is a constant depicting the adsorption intensity, q_{max} (mg/g) is the maximum adsorption capacity of the adsorbent and K_L (L/mg) is the Langmuir adsorption constant. The constants are evaluated from the intercept and slope of a linear plot of the experimental data. The essential characteristics of Langmuir equation can be expressed in terms of the dimensionless separation factor, R_L, defined as:

$$R_L = \frac{1}{1 + K_L C_o} \quad (8)$$

where C_o is the initial dye concentration at which the adsorption isotherm is considered to be favorable ($0 < R_L < 1$), linear ($R_L = 1$), unfavorable ($R_L > 0$) or irreversible ($R_L = 0$) on the basis of R_L. The MB adsorption experimental data were fitted with the Langmuir and Freundlich isotherm models. The obtained parameters from Fig. 6 are tabulated in Table 2.

As evident in Fig. 6(a,b), the Langmuir isotherm models coincide very well with the experimental data; better than the Freundlich isotherm model at both concentrations used. This suggests that active sites are homogeneously distributed on the surface of the adsorbent and the adsorption process is monolayer coverage of the dye on the surface of the CPs. Also, the dimensionless separation factor R_L is said to be favorable, as shown in Table 2.

Selective adsorption

Separation of a particular dye from a solution mixture has important practical applications. Because of the negative surface of the CPs, as evident from Zeta value, it is possible to use CPs for the selective adsorption of cationic dye from a mixture of dyes. The mixture of MB and MO showed characteristic dual absorption peaks at 665 and 463 nm in the UV/vis absorption spectra, as shown in Fig. 7(a). It was noticed that the intensity of the 665 nm band corresponding to MB decreased significantly, whereas no obvious decrease was observed at 463 nm, the characteristic absorption band of MO. This demonstrated the high selectivity of

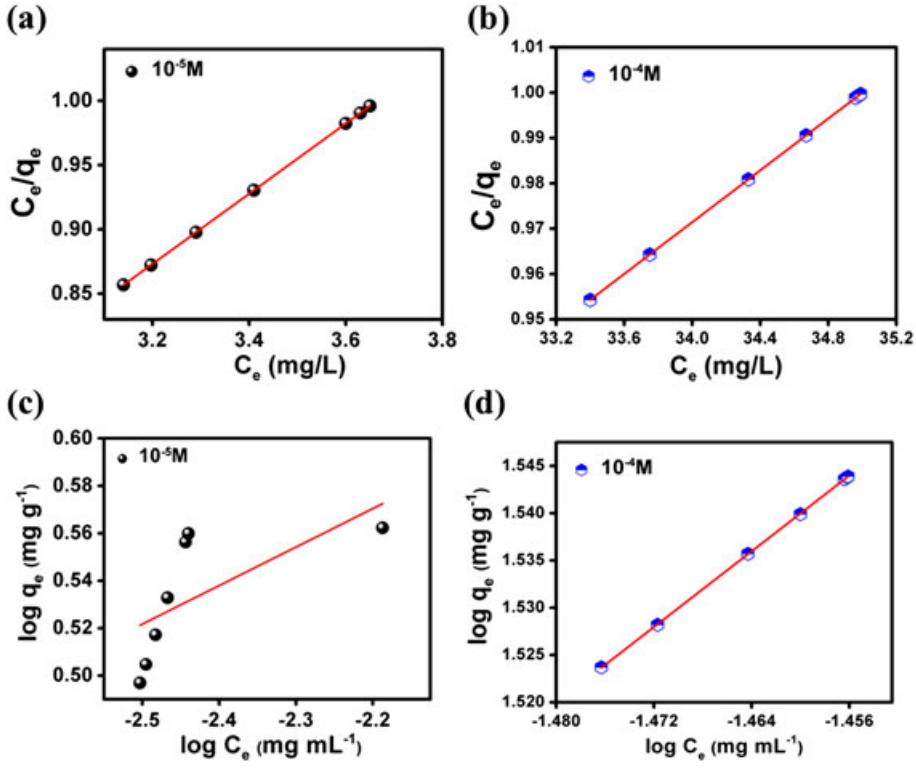

Figure 6. (a, b) Langmuir adsorption isotherm and (c, d) Freundlich adsorption isotherm plots for MB at initial concentrations of 10^{-5} M (a, c) and 10^{-4} M (b, d).

Table 2. Adsorption isotherm parameters for MB adsorption on CPs at initial concentrations of 10^{-5} and 10^{-4} M

	Langmuir isotherm			Freundlich isotherm			
C_o (M)	q_{max} (mg/g)	K_L (g/mL)	R^2	R_L	K_F (mg/g)	b_F (g/mL)	R^2
10^{-5}	3.665	5.08×10^5	1	5.28×10^{-7}	1.4530	0.9274	0.31539
10^{-4}	35.014	1.000	1	0.964	10.033	3.00205	0.9996

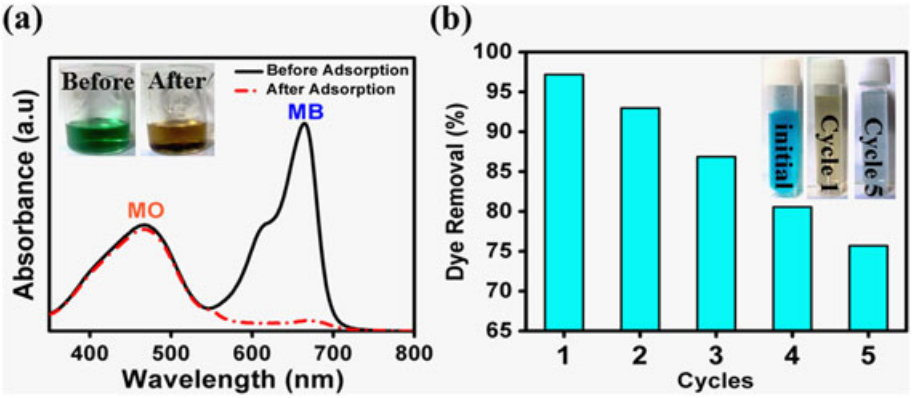

Figure 7. (a) UV absorption spectra of a mixed solution of MB and MO, before and after selective adsorption onto CPs. (Inset) Photograph of a mixed solution of MB and MO before and after selective adsorption onto CPs. (b) Regenerative ability of the CP adsorbents. (Insert) Photographs of aqueous solutions of MB before adsorption, after the first adsorption and after the fifth cycle.

CPs for adsorption of the cationic dye. The high selectivity may be due to electrostatic attraction between the CPs and the dye, which is the main driving force for the adsorption process.

Desorption study

In real-life applications, the regeneration capability of the adsorbent is important because the dyes can be recovered and the adsorbent can be regenerated and reused further. An excellent adsorbent should possess not only a high adsorption ability, but also a high desorption capability in order to significantly reduce the overall cost of the adsorbent. Five cycles of desorption–adsorption were performed with the CPs, as shown in Fig. 7(b). From the regeneration results, it is clear that the adsorption ability of CPs decreased with repeated usage.

Conclusions

A green and economic technique of synthesizing CPs by low-temperature carbonization of a cost-effective and readily available food waste (orange peel precursor), with excellent fluorescent properties and cationic dye adsorption efficiency was successfully demonstrated. The partially crystalline CPs exhibited strong and stable excitation-dependent photoluminescence. Our experimental results showed that stirring at 150 rpm was sufficient for the rapid adsorption of MB dye onto the CPs surface, which exhibited better adsorption at pH 7. Moreover, the extent of dye removal increased with increasing initial dye concentration. The pseudo-second-order kinetics model confirmed the experimental data for both concentrations used. The equilibrium adsorption isotherm showed that the Langmuir model better describes the adsorption process than the Freundlich model. As-prepared CPs rapidly adsorbed ~84% of the MB within 1 min and can be regenerated and used repeatedly. From our results, it is evident that fluorescent CPs not only have bioimaging applications, but also could be used as a low cost, environmentally friendly and promising adsorbent for the efficient removal of cationic dyes from wastewater.

Acknowledgements

OA acknowledges CSIR and TWAS for 2013 TWAS-CSIR postgraduate fellowship AR acknowledges the Department of Science and Technology, Government of India for awarding INSPIRE junior research fellowship to carry out PhD. PSD acknowledges CSIR TAPSUN for the financial support.

References

1. Baker SN, Baker GA. Luminescent carbon nanodots: emergent nanolights. Angew Chem Int Ed 2010;49:6726–44.
2. Luo PG, Sahu S, Yang ST, Sonkar SK, Wang J, Wan H, et al. Carbon 'quantum' dots for optical bioimaging. J Mater Chem B 2013;1:2116–27.
3. Sun Y-P, Zhou B, Lin Y, Wang W, Femando KAS, Pathak P, et al. Quantum-sized carbon dots for bright and colorful photoluminescence. J Am Chem Soc 2006;128:7756–7.
4. Ray SC, Saha A, Jana NR, Sarkar R. Fluorescent carbon nanoparticles: synthesis, characterization and bioimaging application. J Phys Chem C 2009;113:18546–51.
5. Prasannan A, Imae T. One pot synthesis of fluorescent carbon dots from orange waste peels. Ind Eng Chem Res 2013;52:15673–8.
6. Zhou J, Sheng Z, Han H, Zou M, Li C. Facile synthesis of fluorescent carbon dots using watermelon peel as a carbon source. Mater Lett 2012;66:222–4.
7. Liu Y, Zhao Y, Zhang Y. One-step green synthesized fluorescent carbon nanodots from bamboo leaves for copper(II) ion detection. Sensors Actuators B Chem 2014;196:647–52.
8. Huang H, Xu Y, Tang C-J, Chen J-R, Wang A-J, Feng J-J. Facile and green synthesis of photoluminescent carbon nanoparticles for cellular imaging. New J Chem 2014;38:784–9.
9. Park SY, Lee HU, Park ES, Lee SC, Lee J-W, Jeong SW, et al. Photoluminescent green carbon nanodots from food-waste-derived

LUMINESCENCE
The Journal of Biological and Chemical Luminescence

sources: large scale synthesis, properties, and biomedical applications. ACS Appl Mater Interfaces 2014;6:3365–70.
10. Yang ZC, Wang M, Young AM, Wong SY, Zhang XH, Tan H, et al. Intrinsically fluorescent carbon dots with tunable emission derived from hydrothermal treatment of glucose presence of monopotassium phosphate. Chem Commun 2011;47:11615–7.
11. Mewada A, Pandey S, Shinde S, Mishra N, Oza G, Thakur M, et al. Green synthesis of biocompatible carbon dots using aqueous extract of *Trapabispinosa* peel. Mater Sci Eng C 2013;33:2914–7.
12. De B, Karak N. A green and facile approach for the synthesis of water soluble fluorescent carbon dots from banana juice. RSC Adv 2013;3:8286–90.
13. Saxena M, Sarkar S. Synthesis of carbogenic nanosphere from peanut skin. Diam Relat Mater 2012;24:11–4.
14. Yang H, Yan R, Chen H, Zheng C, Lee DH, Liang DT. In the depth investigation of biomass pyrolysis based on three major components: hemicellulose, cellulose and lignin. Energy Fuel 2006;20:388–93.
15. Mohan D, Jr Pittman CU, Steele PH. Pyrolysis of wood/ biomass for bio-oil: a critical review. Energy Fuel 2006;20:849–89.
16. Yang S-T, Luo J, Liu J-H, Zhou Q, Wan J, Ma C, et al. Carbon nanoparticles for cationic dye (methylene blue) removal from aqueous solution. Nanosci Nanotechnol Lett 2012;4:839–42.
17. Tan XW, Romainor ANB, Chin SF, Ng SM. Carbon dots production via pyrolysis of sagowaste as potential probe formetal ions sensing. J Anal Appl Pyrolysis 2014;105:157–65.
18. Wee SS, Ng YH, Ng SM. Synthesis of fluorescent carbon dots via simple acid hydrolysis of bovine serum albumin and its potential as sensitive sensing probe for lead(II) ions. Talanta 2013;116:71–6.
19. Cao L, Wang X, Meziani MJ, Lu F, Wang H, Luo PG, Lin Y, Harruff BA, Veca LM, Murray D, Xie SY, Sun YP. Carbon Dots for Multiphoton Bioimaging. J Am Chem Soc 2007;129:11318–19.
20. Shi H, Li W, Zhong L, Xu C. Methylene blue adsorption from aqueous solution by magnetic cellulose/ grapheme oxide composite: equilibrium, kinetics and thermodynamics. Ind Eng Chem Res 2014;53:1108–18.
21. Yang H, Yan R, Chen H, Lee HD, Zheng C. Characteristics of hemicellulose, cellulose and lignin pyrolysis. Fuel 2007;86:1781–8.
22. Zepata B, Balmaseda J, Fregoso-Israel E, Torres-Garcia E. Thermo-kinetics study of orange peel in air. J Therm Anal Calorim 2009;98:309–15.
23. Ho YS, McKay G. Kinetic models for the sorption of dye from aqueous solution by wood. Trans I Chem E 1998;76:183–91.
24. Weber WJ, Morris JC. Kinetics of adsorption on carbon from solution. J Sanit Eng Div 1963;89:31–60.
25. Wang Q, Li J, Song Y, Wang X. Facile synthesis of high quality plasma reduced graphene oxide with ultrahigh 4,4′-dichlorobiphenyl adsorption capacity. Chem Asian J 2013;8:225–31.
26. Langmuir I. The adsorption of gases on plane surfaces of glass, mica and platinum. J Am Chem Soc 1981;40:1361–403.
27. Freundlich HMF. Over the adsorption in solution. J Phys Chem 1906;57:385–71.

Supporting information

Additional supporting information may be found in the online version of this article at the publisher's web site.